ELSEVIER

Chemical Engineering Journal 137 (2008) 396–410

Chemical Engineering Journal

www.elsevier.com/locate/cej

Optical properties of goethite catalyst for heterogeneous photo-Fenton reactions Comparison with a titanium dioxide catalyst

Guadalupe B. Ortiz de la Plata, Orlando M. Alfano, Alberto E. Cassano *

INTEC (CONICET and Universidad Nacional del Litoral), Güemes 3450, (3000) Santa Fe, Argentina

Received 8 January 2007; received in revised form 2 May 2007; accepted 4 May 2007

Abstract

Optical properties of solid catalysts needed for a rigorous modeling of heterogeneous photo-Fenton reaction kinetics and the ultimate reactor design have not been studied so far. Without these data, quantitative information concerning the influence of the radiation field in the process performance is almost impossible. These reactions are still under the first stages of their studies, and most of the effort has been aimed at elucidate yields, tentative mechanisms, the optimum operating pH and ways to reduce iron ions leaching to the aqueous solution. This work reports the values of above-mentioned parameters precisely calculated, resorting to specially designed spectrophotometer measurements coupled with the solution of the radiative transfer equation (RTE). Goethite, a natural occurring ferric oxide, was studied to obtain the values of the radiation linear volumetric absorption and scattering coefficients, as well as the phase function for scattering, some of them as a function of mass composition, and all of them as a function of the wavelength range between 310 and 500 nm. The results indicate that, in addition to its demonstrated ability to degrade effectively many contaminants, its optical properties exhibit very low absorption and scattering properties. This outcome improves its potentiality for applications in large-scale reactors, because the resulting useful optical path length will be significantly large. Specifically, these results are compared with a typical photocatalytic substance, such as titanium dioxide to remark the differences.

Keywords: Heterogeneous photo-Fenton; Goethite; Optical properties; Radiation field; Comparison with titanium dioxide

1. Introduction

In the last decades, increasing concern has developed regarding the existence of different forms of pollution in both, disposal of domestic discharges or waste emissions from industrial effluents. This problem has given rise to an intensive search for new methods to control environmental pollution. Special emphasis has been placed in those that lead to the total degradation of the undesirable substances and are, at the same time, fast and/or economical. From this last point of view, biological processes have shown to be the most attractive alternative as long as the involved compounds are not refractory to biodegradation or exhibit inadmissible toxicity for the employed microorganisms. As a complement (a pretreatment, for example), a different approach has been introduced in the last few decades under the generic denomination of Advanced Oxidation Technologies (AOT). Most of them, still in the stage of development, have the particularity to transform the existing pollution in innocuous end products, such as carbon dioxide, water and low concentrations of mineral acids. However, sometimes for economical reasons it is not convenient to reach the end of the AOT reactions. Instead, it is advisable to use them in combination with biological processes [1,2]. In the majority of the existing processes, the principal responsible for an effective degradation is the existence of highly reactive $OH^{\bullet}$ radicals. They usually react with very low selectivity permitting the treatment of a large variety of pollutants. These processes include a large family of possibilities, some of them employing UV radiation. Among them, it can be mentioned the use of titanium dioxide + UV, hydrogen peroxide + UV, ozone + UV and finally, hydrogen peroxide with ferric salts + UV with the generic denomination of photo-Fenton processes.

The photo-Fenton process has been widely proposed to degrade many compounds and/or improve the biodegradability of aqueous effluents. It has been found suitable for the treatment of pesticides [3], pharmaceutical wastes [4] and petrochemical

* Corresponding author. Fax: +54 342 4511087.
E-mail address: acassano@ceride.gov.ar (A.E. Cassano).

1385-8947/$ – see front matter © 2007 Elsevier B.V. All rights reserved.
doi:10.1016/j.cej.2007.05.008

Nomenclature

a_n	Legendre expansion coefficient of order n
Abs(...)	absolute value
C_i	concentration of component i (mol cm^{-3})
C_m	catalyst concentration (g cm^{-3})
C^0_{2-CP}	initial 2-chlorophenol concentration (g cm^{-3})
Diff	difference
e^a	local volumetric rate of photon absorption (LVRPA) (Einstein cm^{-3} s^{-1})
EXT	extinctance
fr	relative residuals for the reflectance measurements
ft	relative residuals for the transmittance measurements
g	asymmetry factor
$\bar{g}$	average value of asymmetry factor
G	incident radiation (Einstein cm^{-2} s^{-1})
h	reactor axial coordinate (cm)
I	specific radiation intensity (Einstein sr^{-1} cm^{-2} s^{-1})
L	length (cm)
$\underline{n}$	normal vector
p	phase function
P_n	Legendre polynomial of order n
q	radiative flux (Einstein cm^{-2} s^{-1})
Q	flow rate (cm^3 s^{-1})
R	diffuse reflectance
RTE	radiative transfer equation
s	lineal coordinate along the direction Ω (cm)
S	source term (Einstein sr^{-1}cm^{-3} s^{-1})
t	time (s)
T	diffuse transmittance
TOL	tolerance for the convergence
V	volume (cm^3)
W	cell wall thickness (cm)
x	Cartesian axial coordinate (cm)

Greek letters

α	reaction order
β	volumetric extinction coefficient (cm^{-1})
β^*	specific extinction coefficient (cm^2 g^{-1})
δ	Dirac Delta Function
Γ	global reflection coefficient
θ	spherical coordinate (rad)
θ_0	angle between the direction of incident and scattered rays (rad)
κ	volumetric absorption coefficient (cm^{-1})
κ^*	specific absorption coefficient (cm^2 g^{-1})
λ	wavelength (nm)
μ	cos θ
σ	volumetric scattering coefficient (cm^{-1})
σ^*	specific scattering coefficient (cm^2 g^{-1})
Ω	solid angle (sr)
$\underline{\Omega}$	unit vector in the direction of radiation propagation

Subscripts

0	inlet condition
Cell	relative to the cell
cm	catalyst mass
HG	Henyey and Greenstein phase function
λ	dependence on wavelength
R	relative to the reactor
React.	relative to the reaction
T	relative to the Tank
$\sum_\lambda \lambda$	polychromatic radiation

Superscripts

*	specific property
+	forward direction
−	backward direction

wastes [5]. Different groups, among which the important contributions of Sun and Pignatello [6], Bossmann et al. [7], De Laat and Gallard [8] and Pignatello et al. [9] can be cited, have tried the elucidation of the involved mechanism. Application of the reaction using solar radiation has also been reported, for example by Malato et al. [10] and Rossetti et al. [11] which provide and additional incentive for its use. Interestingly, in the last decade research has been particularly oriented to search for the immobilization of iron compounds in different supports to work with larger size particles in order to avoid the otherwise necessary downstream posttreatment to separate the dissolved iron compounds existing in the homogeneous operation. Hence, heterogeneous photo-Fenton reactions have started a new group of AOT and numerous proposals can be found in the scientific literature, such as membranes [12–14], alginates [15], silica [16,17], zeolites [18–20], clays [21,22], alumina [23], activated carbon [24], natively found iron oxides [23,25,26], and iron-containing SBA-15, a novel mesoporous and active photo-Fenton catalyst [27,28]. With a few exceptions, the search for high yields, plausible mechanisms, optimum operating pHs and suppression of the undesirable leaching of iron to the solution, have been the most important problems addressed in these studies. In some cases, reaction times are still too large, a hindrance that is sheared with many of the supported titanium oxide proposals to treat water environmental problems. With respect to the quoted groups in the next to the last list of references, very important additional information have been made concerning the use of goethite as a catalyst, providing evidences about its suitability for the Fenton and photo-Fenton reactions, and suggesting possible reaction mechanisms ([26,29–37], among others). On the other hand, quantitative kinetic studies aimed at providing working kinetic models for reactor design purposes have been very scarce.

Whichever the type of employed catalyst and the eventual reaction mechanism that is associated with the involved process, in all photo-Fenton cases, a photochemical step will exist. Then, for the development of the reaction kinetics, the correct evaluation of the photon absorption rate (the local volumetric rate of photon absorption or the LVRPA) will be always required.

In all cases, this step cannot be precisely calculated if the optical properties of the employed radiation absorbing species are not known. The problem has significantly increasing difficulties in heterogeneous systems employing solid catalysts due to the presence of light scattering. In this case, the problem is solved with the application of the complete radiative transfer equation (RTE). In this equation, there are two parameters and one function that must be previously known to apply the RTE to each particular case. They are: (i) the linear volumetric absorption coefficient, (ii) the linear volumetric scattering coefficient and (iii) the phase function that describes the spatial characteristics of the scattering phenomenon. This leads to the conclusion that there exists an unavoidable need to know the above-mentioned parameters and the phase function for solid catalyst, such as iron oxides. Some of these features have been roughly estimated for dry goethite samples in air, using the old and approximate method proposed in the Kubelka–Munk model [38,39].

The proposed solution to the above-described problem can be illustrated with a commendable, above-mentioned catalyst candidate, such as goethite, which combines some of the required properties for large-scale applications: (i) photocorrosion resistance, (ii) wide range of operating pHs and, specially (iii) an almost undetectable leaching of iron into the solution. Studies on the use of goethite have been stimulated by different factors: (i) it is one of the most chemically active compounds suspended in natural waters, (ii) it is one of the most common forms of iron oxides found in oxisoils of temperate regions, (iii) it is considered one of the most environmentally friendly catalysts; (iv) it has a low prize because it is broadly found in nature, (v) it has a very high thermodynamic stability, (vi) it has a low energy requirement, (vii) it is widely used as a model compound in soil remediation, (viii) its catalytic activity is quite acceptable and (ix) it can be operated with solar radiation.

This work is aimed at two main objectives: (1) to obtain the characterization of the optical properties of goethite in practical sizes for efficient operating conditions (good chemical activity, possibility of suspension uniformity under powerful stirring – or high flow rate in continuous systems – and settling facility under stagnant conditions) and (2) to compare its properties with the well-known titanium dioxide in order to analyze its advantages or difficulties for photoreactor design.

2. The model for the radiant field

The central experimental method to accomplish the first objective is based on a rigorous modeling of the performance of two components of a typical UV-visible spectrophotometer: the sampling cell and an integrating sphere. In this way, it will be possible to interpret the experimental outcomes in a non-conventional manner and reach the desired results. Consequently, the first step is to develop the mathematical fundaments that will be required to carry out the proposed modeling. Simultaneously, it will serve to show, in a straightforward manner, the way that the same fundamentals must be used to calculate the LVRPA.

For rather dilute suspensions (concentration of solids smaller than 5–10%) a pseudo-homogeneous three-dimensional model of the radiant field along a single direction of propagation in the three-dimensional space, can be described by the following general equation for radiative transport [40,41]:

$$\frac{\mathrm{d}I_{\lambda,\underline{\Omega}}(s,t)}{\mathrm{d}s} + \underbrace{\kappa_\lambda(s,t)I_{\lambda,\underline{\Omega}}(s,t)}_{\text{absorption}} + \underbrace{\sigma_\lambda(s,t)I_{\lambda,\underline{\Omega}}(s,t)}_{\text{out-scattering}} = \underbrace{\frac{\sigma_\lambda(s,t)}{4\pi}\int_{\Omega'=4\pi} p_\lambda(\underline{\Omega}'\rightarrow\underline{\Omega})I_{\lambda,\underline{\Omega}}(s,t)\,\mathrm{d}\Omega'}_{\text{in-scattering}} \quad (1)$$

where $\mathrm{d}I_{\lambda\underline{\Omega}}(s,t)/\mathrm{d}s$ is the rate of change of the spectral specific intensity measured along the directional coordinate s, having a wavelength λ (between λ and $\lambda+\mathrm{d}\lambda$) and a direction of radiation propagation characterized by the unit vector $\underline{\Omega}$. Emission has been neglected because photocatalytic reactions are performed at ambient temperature and all other forms of induced emission are non-existent. κ_λ and σ_λ are the absorption and scattering linear volumetric coefficients and p is the phase function for elastic scattering that acts as a source of photons coming from any direction $\underline{\Omega}'$ to the direction under consideration $\underline{\Omega}$.

Once the spectral and directional distribution of radiation intensities is known by solving Eq. (1), the spectral incident radiation that results from the integration of the specific intensities from all the contributing directions of radiation propagation ($\underline{\Omega}$) to the point under consideration located at position $\underline{x}$ can be readily calculated according to:

$$G_\lambda(\underline{x},t) = \int_\Omega I_{\lambda,\underline{\Omega}}(\underline{x},t)\,\mathrm{d}\Omega \quad (2)$$

From Eq. (2), the important property responsible for activating the catalyst, the spectral local volumetric rate of photon absorption is obtained as follows:

$$e^a_\lambda(\underline{x},t) = \kappa_{\lambda,\mathrm{React.}}(\underline{x},t)G_\lambda(\underline{x},t) \quad (3)$$

In addition, for polychromatic radiation:

$$e^a_{\sum_\lambda}(\underline{x},t) = \int_{\lambda_1}^{\lambda_2}\kappa_\lambda(\underline{x},t)G_\lambda(\underline{x},t)\,\mathrm{d}\lambda \quad (4)$$

where the subscript React. includes two possibilities: (i) a chemically active species capable of absorbing radiation and initiating a reaction and (ii) a catalyst with the quality of being able to become activated by the appropriate radiation absorbing process. The value of $e^a_{\sum_\lambda}(\underline{x},t)$ intervenes in every kinetic expression describing kinetically controlled photochemical reactions. Thus, the solution of the RTE [Eq. (1)] is the first step to calculate Eq. (4).

It is clear that to solve the RTE inside the reactor to calculate the LVRPA, the absorption coefficient κ_λ (s,t), the scattering coefficient σ_λ (s,t) and the phase function $p_\lambda(\underline{\Omega}'\rightarrow\underline{\Omega})$ must be known. This constitutes a more precise definition of the first objective of this contribution. Thus, it is necessary an accurate measurement of these properties that are indispensable for quantitative reaction kinetic studies as well as for reactor design using mathematical modeling. At the same time, this information will permit to realize the second objective and compare the

characteristics of the chosen iron oxide (goethite) with classical titanium dioxide photocatalysts. In real terms, the approach to reach the described purpose represents the solution of the so-called inverse problem. From specifically designed experimental measurements, Eq. (1) will be applied to the spectrophotometer accessories to estimate the distinctive parameters and functions that characterize the system. Or, in other terms, Eq. (1) will be used to retrieve from a series of three independent measurements performed in a spectrophotometer cell, the values of its three significant parameters and correlate them as a function of the catalyst concentration and wavelength. In this way, specific (per unit mass concentration) physical properties can be obtained as a function of wavelength as well as the wavelength distribution of the scattering phase function. The uniqueness of these results has to be, afterwards, verified analyzing their ability to predict and reproduce all the primitive experimental measurements.

In former determinations of the optical properties of titanium dioxide [42–44] results were reported resorting to plausible assumptions concerning the most convenient phase function to use in Eq. (1). Satuf et al. [45], working with small particles of titanium dioxide (a strong absorbing and scattering substance), have shown that it is possible to design new, additional experiments to remove this assumption and obtain much better information concerning the scattering distribution function.

For this type of experiments, when the incident radiation incoming to the cell from the spectrophotometer radiation source is azimuthally symmetric, the phase function must be first integrated over the angle of symmetry:

$$\int_{\Omega'=4\pi} p(\underline{\Omega}' \rightarrow \underline{\Omega}) I_{\lambda,\underline{\Omega}}(s,t)\,\mathrm{d}\Omega' = \int_{\mu'=-1}^{1} I_\lambda(x,\mu') \left[\int_{\phi'=0}^{2\pi} p(\mu_0)\,\mathrm{d}\phi'\right] \mathrm{d}\mu' \tag{5}$$

This operation requires an expansion of $p(\mu_0)$ in terms of Legendre polynomials [40]. The terms of the expansion are:

$$p(\mu_0) = \sum_{=0}^{N} a_n P_n(\mu_0), \quad a_0 = 1 \tag{6}$$

where μ_0 is the cosine of the angle between the incoming and the scattered ray and P_n are the Legendre polynomials of order n and argument μ_0.

After considering azimuthal symmetry and integrating between $\phi' = 0$ and 2π:

$$\int_{\phi'=0}^{2\pi} p(\mu_0)\,\mathrm{d}\phi' \cong 2\pi \sum_{n=0}^{N} a_n P_n(\mu) P_n(\mu') = 2\pi p(\mu,\mu') \tag{7}$$

For the choice of the phase function, following the work of Satuf et al. [45], the one parameter equation suggested by Henyey and Greenstein, the HG phase function [46] was adopted:

$$p_{\mathrm{HG},\lambda}(\mu_0) = \frac{(1-g_\lambda^2)}{(1+g_\lambda^2-2g_\lambda\mu_0)^{3/2}} \tag{8}$$

In Eq. (8) g_λ is called the dimensionless asymmetry factor, defined as:

$$g_\lambda = \frac{1}{2}\int_{-1}^{1} p_{\mathrm{HG},\lambda}(\mu_0)\mu_0 \mathrm{d}\mu_0 \tag{9}$$

with g_λ to be determined for each particular case. The coefficients to write $p_{\mathrm{HG},\lambda}(\mu_0)$ in terms of an expansion in Legendre Polynomials are given by:

$$a_n = (2n+1)g_\lambda^n \tag{10}$$

The important feature of this phase function is that g_λ can take on values from −1 to 1 passing through 0 which represents the case of isotropic scattering. The negative limit describes a purely reflecting phase function with scattering strongly directed in the backward direction. Conversely, when the positive limit of $g_\lambda = 1$ is approached, the model depicts a scattering mostly pointing towards the forward direction. Thus, with this important modification in the method, it is possible to get, additionally, information about the dimensionless asymmetry factor for the phase function for scattering.

Eq. (1) can be applied to the spectrophotometric cell (Fig. 1a and b) under the following assumptions: (i) the cell is considered to be formed by two infinite plates separated by the cell thickness, (ii) as mentioned before, considering the way in which the spectrophotometer operates (receiving an almost perfectly collimated beam of the incident radiation) the irradiation of the cell can be assumed to exhibit azimuthal symmetry and (iii) the optical properties of the suspension are independent of time and position. Some of these hypothesis, very often forces to perform the experiments and/or interpret the results in a different manner for each type of catalytic particles that is studied.

In these experiments, Eq. (1) is simplified by the azimuthally symmetric radiation beam arriving to the cell [42]. On that account, the analysis of the spectrophotometric cell, can be reduced to a one-dimensional model in space and a one-directional model for radiation propagation. This simplification will be even more properly justified later on, especially in the particular case under consideration, because it will be seen from the experiments that scattering takes on very low values. Thus, the model for the RTE used in the determination of the optical parameters, depends on the actual values of the case under consideration. Sometimes an iteration procedure may be needed. For example, if absorption is not extremely high and scattering is very significant, a two-directional model for radiation propagation will have to be used [47]. With the above assumptions and considering the new form of the phase function, the RTE for the cell becomes:

$$\mu\frac{\mathrm{d}I_{\lambda,\underline{\Omega}}(x,\mu)}{\mathrm{d}x} + \beta_\lambda I_{\lambda,\underline{\Omega}}(x,\mu) = \frac{\sigma}{2}\int_{\mu'=-1}^{1} I_{\lambda,\underline{\Omega}}(x,\mu)\,p(\mu,\mu')\,\mathrm{d}\mu' \tag{11}$$

In Eqs. (5), (7) and (11) $\mu = \cos\theta$, where θ is the angle of radiation propagation after scattering, measured from the Cartesian coordinate x. $\beta_\lambda = \kappa_\lambda + \sigma_\lambda$ is the extinction coefficient (note that in all cases, these parameters have units of cm^{-1}).

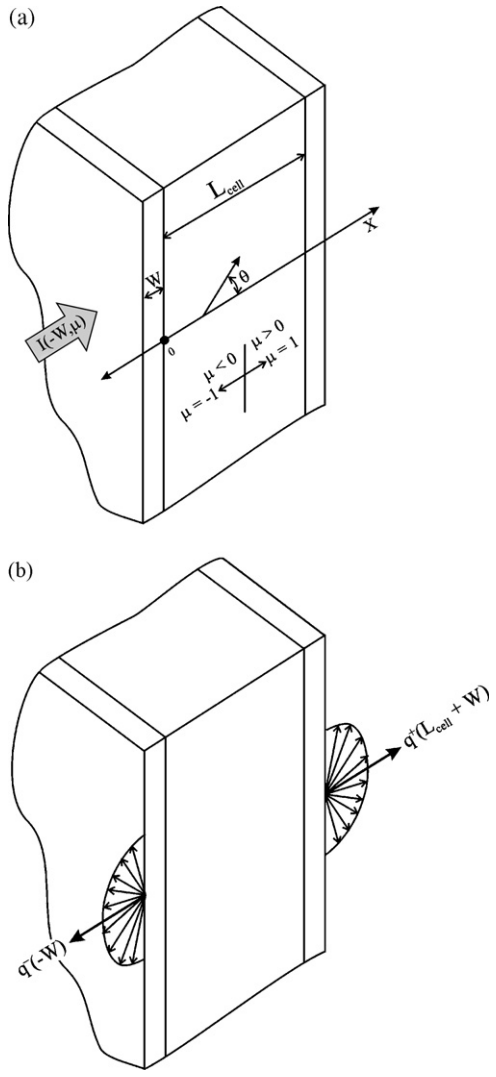

Fig. 1. Schematic representation of the semi-infinite cell.

The walls of the spectrophotometric cell are reflecting surfaces whose influence on the measurements cannot be ignored. They must be incorporated in the boundary conditions. A detailed treatment of the way to calculate these properties can be found in Satuf et al. [45]:

$$I_\lambda(0,\mu) = I_0\delta(\mu-\mu_0) + \Gamma_1 I_\lambda(0,-\mu) \quad (\mu>0) \tag{12}$$

where Γ_1 represents the global wall reflection coefficient corresponding to the radiation that arrives from the internal side of the cell (back-scattering). Note that reflections on the outer side of the cell wall as well as its internal transmission coefficient are taken into account by the blank experiments performed after every single measurement in the spectrophotometer. At the opposite side of the cell (L_{cell}):

$$I_\lambda(L_{cell},-\mu) = \Gamma_1 I_\lambda(L_{cell},\mu) \quad (\mu<0) \tag{13}$$

This model will be used to produce theoretical predictions of the different properties that will be measured and compare them with the results of the corresponding specially designed experiments.

3. Parameters estimation methodology

The approach followed in this work consisted in:

I. Measure the extinction coefficient (β_λ) always as a function of the catalyst concentration and wavelength. These experiments will be called collimated extinctance measurements for reasons that will be apparent below.
II. Calculate the value of the specific extinction coefficient (β^*_λ) with a linear regression with respect to the set of employed catalyst concentrations. The linearity was fully satisfied for the chosen catalyst loadings, comprising all values usually reported in the studies of this reacting system.
III. Employing an integrating sphere, with diffuse transmittance and diffuse reflectance measurements, obtain two independent sets of different experimental values that can be used to extract (from the application of Eqs. (7)–(13) and resorting to a non-linear multiparameter estimator coupled with an optimization program) the value of the absorption coefficient (κ_λ) and the asymmetry factor (g_λ). Once more measurements must be made for different catalyst concentrations and wavelengths. Here, it was necessary to depart from the method developed by Satuf et al. [45]. In the parameter's estimation, the absorption coefficient (κ_λ) has been chosen instead of the scattering coefficient (σ_λ) because of the much higher accuracy obtained in the estimated results employing the first. This particular choice depends on the solid under consideration and it is just opposite to the one adopted when these experiments were made with titanium dioxide [45].
IV. Calculate the specific absorption coefficient (κ^*_λ) by linear regression of the absorption coefficient versus the different employed catalyst concentrations.
V. Calculate, with the values of β^*_λ and κ^*_λ, the specific scattering coefficients (σ^*_λ) that will also be a function of wavelength.
VI. Calculate the dimensionless asymmetry factor as a function of wavelength.

In what follows, the needed experimental information will be described briefly indicating when corresponds, the differences with the method employed in reference [45]. Afterwards, a concise account of the solution of the RTE will be given. In this section, it will be shown the way that the outcomes of the numerical solution can be employed in order to be compared with the experimental results (that do not always give directly the sought parameters). Finally, in Section 7 it will be explained the way to extract from both, experiments and calculated results, the absorption and scattering coefficients and the asymmetry factor.

4. Characteristics of the employed catalyst and reactant

Goethite is a ferric oxide with the following composition: α-FeOOH. The one used in this work was provided by Aldrich in a powder form (LOT05002DC). As received from the supplier it comprises diameters from approximately 0.04 to 0.2 mm. Their respective densities vary from 4.6 to 4.0 g cm^{-3} and the surface

area from 215 to 195 $m^2\,g^{-1}$ according to the size [32]. This author did an extensive study of the influence of the particle size in the rate of the Fenton reaction and found that the reaction rate increases when moving from 70–80 mesh to 200–325 mesh sizes, the reason being that more active surface area is available. However, almost no significant differences between the last and an intermediate size between 100 and 200 mesh were found. A similar but less specific result was observed by Lin and Gurol [30]. In photo-Fenton reactions, it should be expected a similar behavior concerning the dark reaction steps. On the other hand, the optimal situation, as far as light penetration for activating the catalytic particle, should be obtained with the smaller size unless very strong scattering is present. At any rate, it was necessary to decide between the best operating conditions for the reaction and the possibilities of a fast settling process after the reaction is completed. Experimentally, it was found that a good compromising solution was obtained with particles in the size between 100 and 200 meshes (further, an illustrative set of results will be discussed). In this range the reaction has an acceptable yield working with low power black light lamps (input power equal to 18 W) and above 200 mesh settling was definitely too slow.

The suspensions were prepared with bi-distilled, deionized water and the chosen range of particle size (100–200 mesh) made necessary to introduce some modifications in the work performed by Satuf et al. [45] in order to obtain reproducible results in all the spectrophotometer runs, because the suspension stability and the optical properties were very different. Other experimental conditions will be described along the explanation of the required experimental information for the parameter's estimation.

At this point, it was necessary to decide about the model compound for the test, because it has a direct influence on the medium pH and the optical properties have a marked dependence on its value. Considering the available information in the previously quoted references regarding this solid catalyst, it was decided to select as a model compound 2-chlorophenol, provided by Aldrich (reagent grade, ≥99%).

5. Experiments

Measurements of collimated transmittance, diffuse transmittance and diffuse reflectance were made with suspensions of goethite employing different catalyst concentrations [(0.5, 1.0, 1.5, 2 and 2.5) × 10^{-3} g cm^{-3}] and working with twenty equally separated wavelength intervals between 310 and 500 nm. Absorption of ferric oxides extends beyond this value but the corresponding photon energy results very low. These suspensions have a very rapid velocity of sedimentation. With these particles, the procedure employed in reference [45] was not possible. In order to keep the stability of the solid concentration in the cell during the measurements, a recirculating system has to be used, such as, resorting to controlling the suspension flow rate, the mixture of water and the catalyst in the cell had a stable concentration, i.e., the size and density of the particles forced the use of a system of specially adapted flow cells, connected to an outside reservoir equipped with a stirrer and translate the well mixed suspension to the cell with the aid of a pump. Stirring the reservoir had to be made with special care in order to avoid changes in the particle size distribution due to attrition. Measurements were made after one hour of stabilization of the initial readings in the spectrophotometer (reproducing what should be the starting point of future kinetic measurements, where steady state conditions in all the controlled variables are necessary). In order to confirm the reliability of the performed measurements, for each concentration and each wavelength, measurements were repeated every 3 min, i.e., they were triplicated. It may be noticed that, according to the employed catalyst concentrations, the different components of the device were adjusted to provide the best operating conditions for getting the most accurate results.

5.1. The extinction coefficient

The extinction coefficient ($\beta_\lambda = \kappa_\lambda + \sigma_\lambda$) is a property of the solid suspensions in water that can be directly measured with extinctance experiments. Spectral extinctance [$EXT_\lambda = EXT_\lambda(C_{cm})$] is an almost conventional measurement of spectral Absorbance in homogeneous systems, when the apparatus is modified in such a way that those collimated rays coming from the spectrophotometer source, after traveling through the spectrophotometer cell, emerge in an almost single direction and are captured by the detector preserving a single direction of reception, i.e., excluding as much as possible out- and in-scattering of the out coming rays escaping from the cell and reaching the detector. The definition is a clear extension of the well-known absorbance property for homogeneous systems. Differing from previous work, no limitation in the characteristic length of the cell were imposed, allowing for the existence of very highly or, conversely, poorly absorbing or scattering suspensions. As said before, their values are also dependent on the pH of the medium, the reason being that according to its value, the catalytic particles can undergo agglomeration that strongly affects the optical properties of the suspension, especially around the isoelectric point.

For each catalyst concentration and each wavelength the spectral extinctance is obtained from the following equation:

$$\beta_\lambda = \frac{2.303\,EXT_\lambda}{L_{cell}} \tag{14}$$

where the apparent extinctance is obtained from:

$$EXT_\lambda = -\log T_\lambda = -\log \frac{I_\lambda}{I_{0,\lambda}} \tag{15}$$

With the data of the extinction coefficients for different catalyst concentrations it is possible to obtain immediately the specific extinction coefficients (in units of $cm^2\,g^{-1}$) as a function of wavelength.

5.2. The absorption coefficient and the asymmetry factor

To calculate these properties two independent experiments are needed. The first is a diffuse transmittance assay that collects all the rays coming from the cell in the forward direction

(including all forms of scattering from all directions) and the second, a diffuse reflectance measurement that provides exclusively information concerning the reflectance of the suspension. Note that in the first case all the forwardly transmitted (unabsorbed) radiation through the cell were also collected.

The results are analyzed resorting to the solution of the RTE and comparing theoretical predictions (obtained from the adopted initializing values of the parameters employed to perform the calculations) with the experimental data. At this point it was necessary to resort to the previously described non-linear multiparameter estimator. The corresponding obtained experimental measurements, as illustrated by Fig. 1b are:

$$T_\lambda = \frac{q_\lambda^+(L_{\text{cell}} + W)}{q_\lambda^+(-W)} \tag{16}$$

$$R_\lambda = \frac{q_\lambda^-(-W)}{q_\lambda^+(-W)} \tag{17}$$

Considering the definition of the radiation flux,

$$\underline{q}_\lambda(\underline{x}) = \int_{\Omega=4\pi} \mathrm{I}_{\lambda,\underline{\Omega}}(\underline{x})\underline{n}\,\mathrm{d}\Omega \tag{18}$$

the following equations result:

$$q_\lambda^+(-W) = 2\pi \int_0^1 \mu I_\lambda(-W, \mu)\,\mathrm{d}\mu \tag{19}$$

$$q_\lambda^-(-W) = 2\pi \int_{-1}^0 \mu I_\lambda(-W, \mu)\,\mathrm{d}\mu \tag{20}$$

$$q_\lambda^+(L + W) = 2\pi \int_0^1 \mu I_\lambda(L + W, \mu)\,\mathrm{d}\mu \tag{21}$$

The experimental values are compared with the results produced by the solution of the RTE as explained below. More details are given in Satuf et al. [45].

6. Solution of the RTE

To solve this integro-differential equation (the RTE) it is possible to resort to a precise numerical procedure, known as the discrete ordinate method (DOM) [48], originally developed for neutron transport. Although the RTE can be analytically solved in very restricted cases (isotropic scattering and flat, one-dimensional geometries) and other methods of solution also exist, such as Monte Carlo Techniques [49–51], the DOM is recognized as one of the most precise methods available today in spite of some of its difficulties in cylindrical geometries. The quality of the results obtained with this method has been extensively demonstrated [52–55]. To obtain the solution, three different discretizations must be made: (i) the wavelength discretization (the problem must be solved for each different wavelength), (ii) the spatial discretization in the x dimension and (iii) the angular discretization in the θ direction, represented by the variable μ. The conceptual idea is represented in Fig. 1a and b for the last two operations. In essence, Eqs. (7)–(13) must be solved starting from plausible initializing values. Afterwards, compare the theoretical results produced by the model for diffuse transmittance and diffuse reflectance with the experimental values, using the non-linear multiparameter estimator based on the algorithm of Levenberg–Marquardt [56,57]. With this information, at the end of the procedure, κ_λ and g_λ can be obtained. The value of g_λ is equivalent to the knowledge of the required phase function p_λ. The value of σ_λ is obtained by taking the difference of the absorption coefficient from the extinction coefficient (β_λ) resulting from the collimated transmittance measurements.

However, in order to compare the theoretical estimations from the model with the experimental measurements, the results of the DOM in terms of spectral specific intensities must be transformed into radiation fluxes. With this purpose, consider now the dot product of the outwardly directed, unit normal vector corresponding to the surface of radiation entrance to the cell with the radiation flux vector. Then, for the monochromatic, one-dimensional – one-directional radiation model it is obtained that:

$$q_\lambda(x) = 2\pi \int_\mu I_\lambda(x, \mu)\mu\,\mathrm{d}\mu \tag{22}$$

The employed algorithms are illustrated in Figs. 2 and 3. They lead to the information necessary to compare calculated and experimental values of R_λ and T_λ. To simplify notation let us call:

$$I_\lambda(x_{i+1/2}, \mu_m) = I_{\lambda,m}^{i+1/2} \tag{23}$$

Those photons that move forward are represented by:

$$I_{\lambda,m}^{i+1/2} = I_{\lambda,m}^{i-1/2}\frac{\mu_m/\Delta x_i - \beta_\lambda(1-\gamma)}{\mu_m/\Delta x_i + \beta_\lambda\gamma} + \frac{S_{\lambda,m}^i}{\mu_m/\Delta x_i + \beta_\lambda\gamma} \quad (\mu > 0) \tag{24}$$

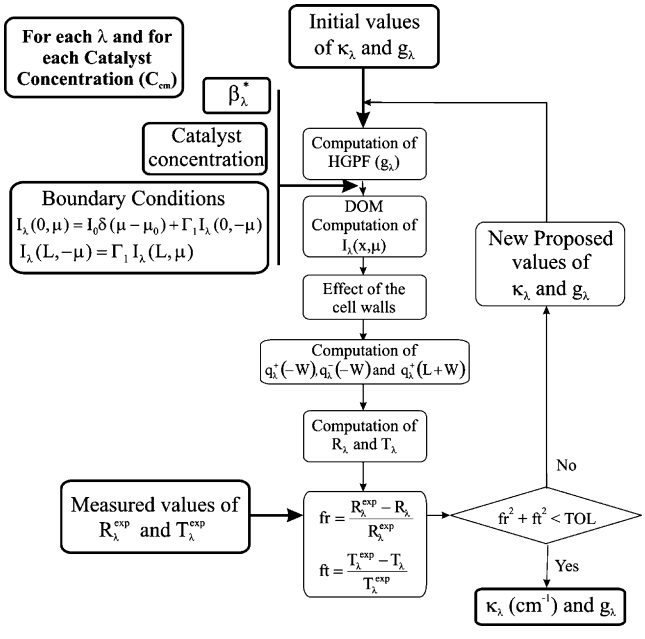

Fig. 2. Parameter estimation algorithm. Part 1.

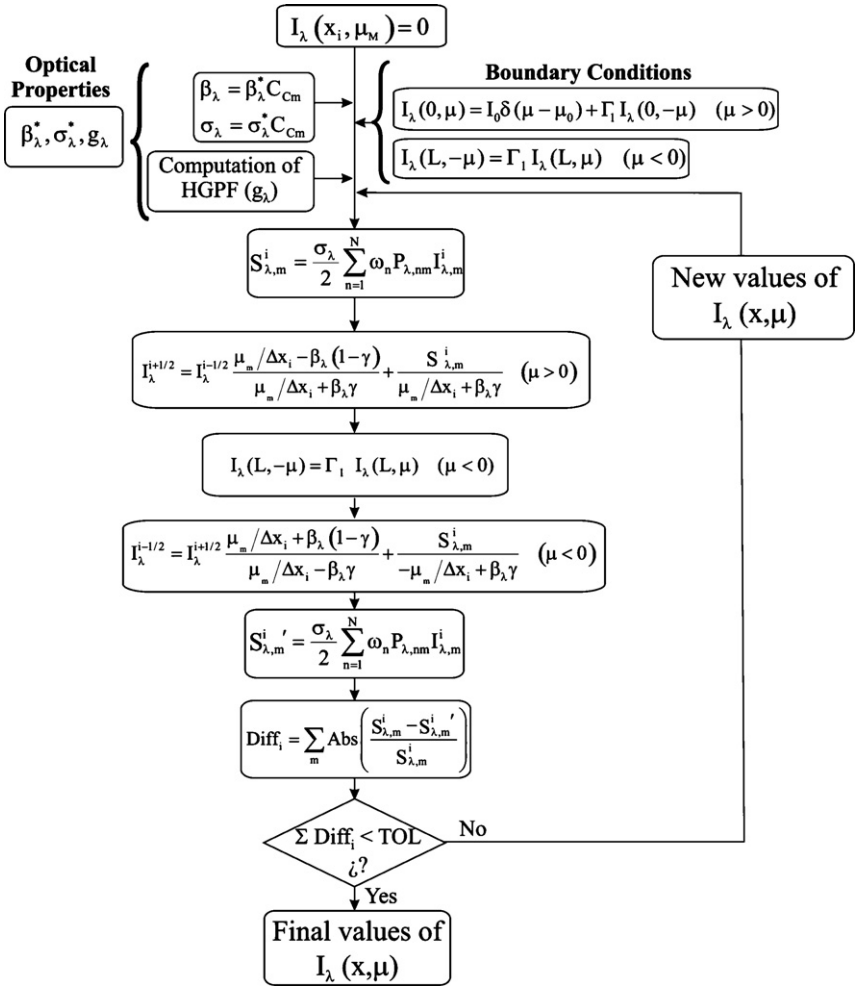

Fig. 3. Parameter estimation algorithm. Part 2.

And those that move backwards:

$$I_{\lambda,m}^{i-1/2} = I_{\lambda,m}^{i+1/2}\frac{\mu_m/\Delta x_i + \beta_\lambda(1-\gamma)}{\mu_m/\Delta x_i - \beta_\lambda\gamma} + \frac{S_{\lambda,m}^i}{-\mu_m/\Delta x_i + \beta_\lambda\gamma} \quad (\mu < 0) \tag{25}$$

In Eqs. (24) and (25) γ is a parameter that, in the numerical method, is equal to 1 if the intensity is negative when calculations are made going in direction and is equal to 0 when calculations are made in the backward direction.

The interpolation between two near points in the source term is made according to:

$$I_\lambda^i = I_\lambda^{i+1/2}\gamma + I_\lambda^{i-1/2}(1-\gamma) \quad \left(\gamma = \frac{1}{2}\right) \tag{26}$$

Calculation of the source term employing a Gaussian quadrature is made in terms of [48]:

$$S_{\lambda,m}^i = \frac{\sigma_\lambda}{2}\sum_{n=1}^{N}\omega_n p_{\lambda,nm} I_{\lambda,n}^i \tag{27}$$

Eq. (27) must be recalculated several times, which forces to resort to an iterative procedure. Usually the procedure starts considering all the intensities equal to zero with the exception of those corresponding to the boundary conditions, and define a tolerance variation for the accuracy of the desired results, according to:

$$\text{Diff}_i = \sum_m \text{Abs}\left(\frac{S_{\lambda,m}^i - S_{\lambda,m}^{i'}}{S_{\lambda,m}^i}\right) \tag{28}$$

The prime value is the result of the last iteration that followed the unprimed value.

7. Results

The first measurements were always those related to collimated transmittance. For each wavelength, employing the values obtained for the different catalyst concentrations, a linear regression was made between extinction coefficients values and catalyst loadings. Fig. 4 shows the values for two different wavelengths. The results of specific extinction coefficients are shown in Fig. 5 and Table 1 (values of two varieties of titanium dioxide are shown for comparison purposes). It can be observed that there are not large fluctuations in the specific extinction coefficient values as a function of wavelength.

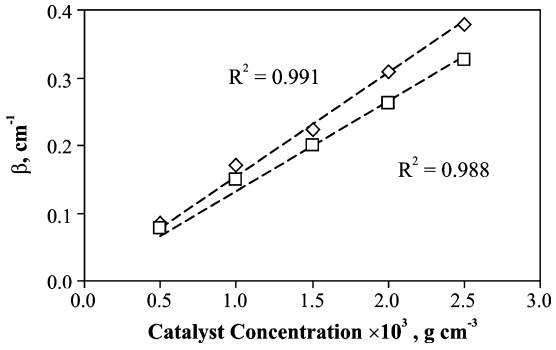

Fig. 4. Portrait of the linear regression to calculate specific extinction coefficients of goethite for two different wavelengths. Diamonds are for λ = 370 nm and squares for λ = 310 nm.

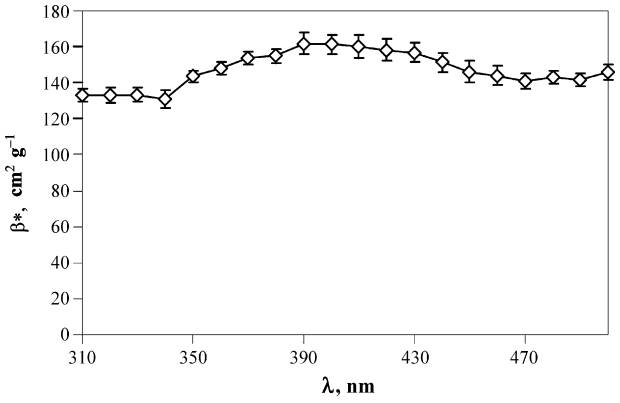

Fig. 5. Specific extinction coefficient of goethite as a function of wavelength.

With the results obtained by comparing the predictions produced by the theoretical model with the experimentally observed values of diffuse transmittance and diffuse reflectance measurements, the values of κ_λ and g_λ were obtained. For these values

Table 1
Specific extinction coefficients as a function of wavelength, β^*_λ(cm^2 g^{-1})

λ (nm)	Goethite	R^2 for goethite	Aldrich[a]	Degussa P 25[a]
310	133	0.99	35754	68464
320	133	0.99	36175	69770
330	133	0.98	36901	69026
340	131	0.98	37844	65395
350	143	0.99	38876	61249
360	148	0.99	39850	57227
370	153	0.99	40538	53200
380	155	0.99	41101	49652
390	161	0.97	41839	46535
400	161	0.98	42509	43707
410	160	0.96	–	–
420	158	0.97	–	–
430	157	0.98	–	–
440	151	0.98	–	–
450	146	0.97	–	–
460	144	0.97	–	–
470	141	0.98	–	–
480	143	0.99	–	–
490	142	0.99	–	–
500	146	0.99	–	–

[a] Taken from Satuf et al. [45].

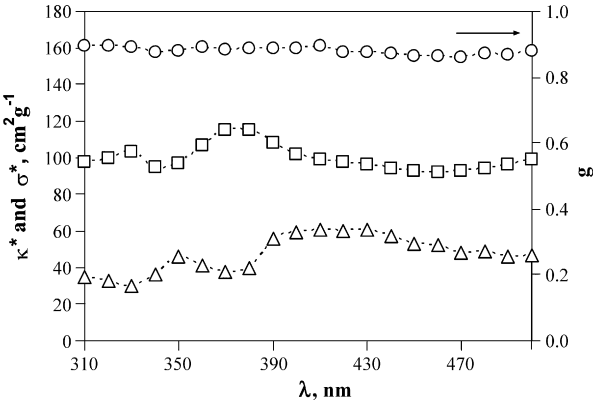

Fig. 6. Specific absorption and scattering coefficients as well as asymmetry factor values as a function of wavelength. Squares are absorption coefficients, triangles scattering coefficients and circles correspond to the dimensionless asymmetry factor.

of κ_λ, and for each wavelength, it is possible to repeat the linear regression as a function of the catalyst concentration. These calculations render the values of κ^*_λ. Knowing the value of β^*_λ, it is very simple to obtain the one corresponding to σ^*_λ. The results of κ^*_λ, σ^*_λ and g_λ are shown in Fig. 6 and Table 2 (again values of the two different varieties of titanium dioxide are also shown). In all cases the value of the asymmetry factor indicates a clear preference for forward scattering. From this point of view the performance of goethite is not very different than titanium dioxide with the exception of the existence of a much moderate dependence with respect to wavelength.

Fig. 7 is a very sensible test to the employed methodology. It compares values of the total measured diffuse transmittance and total measured diffuse reflectance as a function of wavelength with the values obtained from the predictions of σ^*_λ, κ^*_λ and g_λ applying the methodology described in Figs. 2 and 3. It is clear that the optimization program has reached the correct values because employing the calculated values of κ^*_λ, σ^*_λ and g_λ it is possible to predict the original experimental data from 310 to 440 nm with great accuracy. For values between 440 and 500 nm, the diffuse reflectance measurements are so low that the quality of the experimental determinations is significantly decreased and the differences between them and the predictions from the model are less satisfactory.

It can also be observed in Fig. 6 that there is a small variation between the different values of the spectral dimensionless asymmetry factor as a function of wavelength. This observation could induce to use an average value of $g_\lambda = \bar{g}$ in all calculations [47]. Employing a single value of $\bar{g} = 0.887$ the absorption and scattering coefficients were recalculated. No significant differences can be observed comparing the total diffuse transmittance measured and the new calculated values with the simplification previously described. This should be an expected result. Also, this simplification, reproduces with almost the same degree of accuracy the experimental values corresponding to the diffuse reflectance experiments as it can be seen in Fig. 7. The results obtained from these measurements indicate the accomplishment of the first objective.

Table 2
Absorption and scattering coefficients as well as the asymmetry factor as function of wavelength for different catalysts

λ (nm)	Goethite				Aldrich[a]			Degussa P 25[a]		
	κ_λ^* (cm^2 g^{-1})	σ_λ^* (cm^2 g^{-1})	g_λ	R^{2b}	κ_λ^* (cm^2 g^{-1})	σ_λ^* (cm^2 g^{-1})	g_λ	κ_λ^* (cm^2 g^{-1})	σ_λ^* (cm^2 g^{-1})	g_λ
310	98	35	0.897	0.9894	18304	17720	0.8295	37518	30946	0.6925
320	100	33	0.894	0.9860	18307	17869	0.8296	35581	34189	0.6795
330	103	30	0.891	0.9895	18309	18862	0.8065	30326	38700	0.6521
340	95	36	0.875	0.9818	16645	21199	0.7491	22719	42676	0.6151
350	97	46	0.881	0.9901	13589	25287	0.6626	16032	45217	0.5801
360	107	41	0.891	0.9875	8489	31361	0.5569	10708	46519	0.5468
370	115	38	0.883	0.9928	3443	37096	0.4649	6626	46574	0.5161
380	115	40	0.887	0.9895	860	40242	0.4002	3909	45744	0.4878
390	108	56	0.888	0.9729	183	41657	0.3735	1905	44631	0.4612
400	102	59	0.888	0.9839	100	42410	0.3803	745	42963	0.4375
410	99	61	0.894	0.9937	–	–	–	–	–	–
420	98	60	0.875	0.9905	–	–	–	–	–	–
430	96	61	0.876	0.9801	–	–	–	–	–	–
440	94	57	0.873	0.9606	–	–	–	–	–	–
450	93	53	0.863	0.9727	–	–	–	–	–	–
460	92	52	0.866	0.9515	–	–	–	–	–	–
470	93	48	0.860	0.9209	–	–	–	–	–	–
480	94	49	0.871	0.9137	–	–	–	–	–	–
490	96	46	0.868	0.9253	–	–	–	–	–	–
500	99	47	0.878	0.9103	–	–	–	–	–	–

[a] Data extracted from Satuf et al. [45].
[b] The value of R^2 corresponds to the calculation of κ_λ^*.

8. Considerations concerning reactor design

Along this study, an additional, very important and distinctive feature of this catalyst can be observed: its optical characteristics are very different from those of Titania. These differences are shown in Tables 1 and 2 for goethite and two different types of titanium dioxide catalyst. The use of the iron compound should permit a much flexible selection of the reactor dimensions and configurations due to the striking differences observed in the tables. It is well known that in water environments, and employing efficient catalysts concentrations, titanium dioxide give rise to important restrictions on the useful thickness of a practical reactor. The importance of these differences with goethite will be shown in what follows.

To demonstrate in a more convincing way this feature, the following experiments were carried out using 2-chlorophenol as a model compound. The work was performed in a cylindrical, perfectly stirred, batch reactor irradiated from a transparent to radiation bottom that was illuminated with a tubular lamp placed at the focal axis of a parabolic reflector (Fig. 8). Goethite and

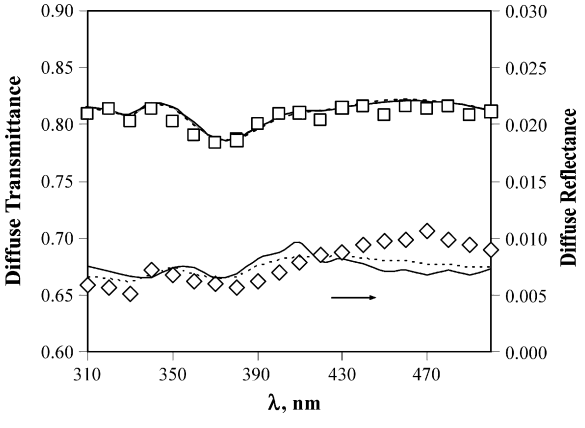

Fig. 7. Validation of the calculation procedure, comparing predicted and measured values of a goethite catalyst for a loading of 2×10^{-3} g cm^{-3}. Squares: measured diffuse transmittances and diamonds: measured diffuse reflectances. Solid lines, in both cases, represent the values predicted with the calculated procedure described in Figs. 2 and 3. Broken lines, in both cases, represent the values predicted with the calculated procedure described in Figs. 2 and 3 employing a constant asymmetry factor.

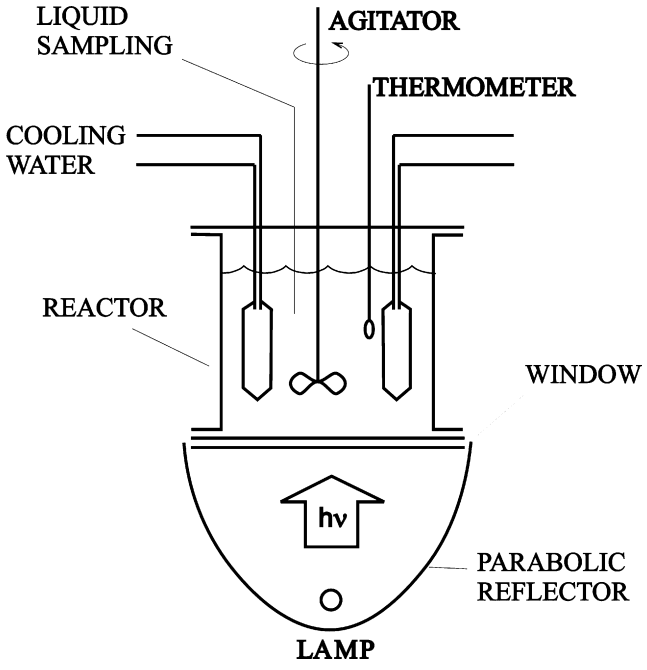

Fig. 8. Schematic representation of the experimental reactor.

Table 3
Characteristics of the reactor for experiments with titanium dioxide and goethite

Characteristics	
Reactor type	Cylindrical, well-stirred batch, with transparent bottom
Main characteristic dimension	Operating depth = 9 cm
Reactor inner diameter	17 cm
Reactor volume	2000 cm^3
Reactor bottom made of	Acrylic/borosilicate glass
Lamp (one)	Tubular, located at the focal axis of a parabolic reflector
Lamp type	TL'D 18W/08
Nominal input power	18 W
Emission range of the lamp	340–420 nm
Lamp diameter	2.6 cm
Lamp length	59 cm
Reflector	Parabolic cylinder
Incident radiation at the reactor bottom	5.55×10^{-9} Einstein $s^{-1} cm^{-2}$

Table 4
Reactor operating conditions

Catalysts	Goethite (from Aldrich)	Titanium dioxide (from Aldrich)
Catalyst concentration	2×10^{-3} g cm^3	2×10^{-3} g cm^3
2-Chlorophenol initial concentration	50 ppm	50 ppm
Hydrogen peroxide concentration	20 mM	–

titanium dioxide, both from Aldrich, were employed. The characteristic of the reactor and the operating conditions are shown in Tables 3 and 4.

Fig. 9 shows the results obtained with both catalysts utilizing two different forms of concentration measurements: (1) 2-chlorophenol disappearance and (2) total organic carbon decay. It is clear that the performance of the heterogeneous photo-Fenton reaction is better. It could be argued that using Degussa P

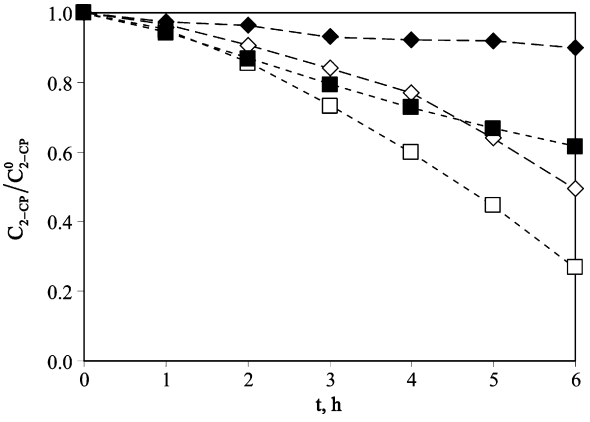

Fig. 9. Experimental results of 2-chlorophenol degradation as a function of time. Black diamonds: TOC concentration employing Aldrich titanium dioxide. Black squares: 2-chlorophenol concentration employing Aldrich titanium dioxide. Void diamonds: TOC concentration employing Aldrich goethite + hydrogen peroxide. Void squares: 2-chlorophenol concentration employing Aldrich goethite + hydrogen peroxide.

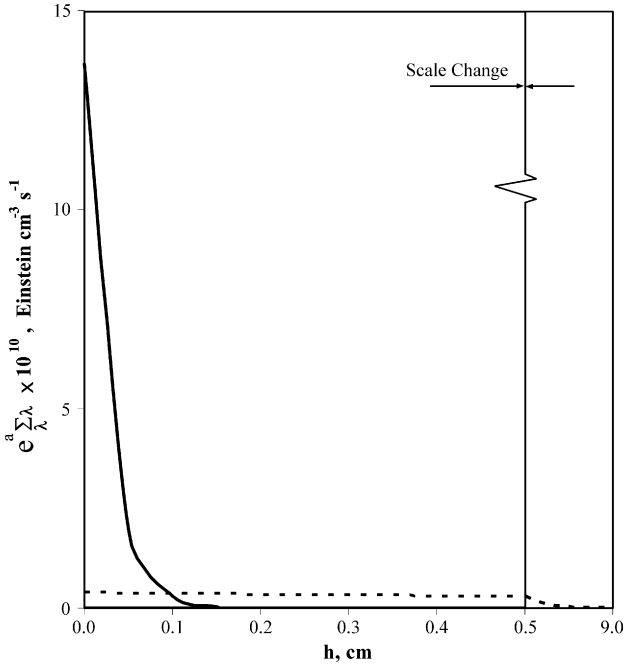

Fig. 10. Calculated spatial distribution of the LVRPA as a function of the characteristic direction of radiation propagation for a loading of 2×10^{-3} g cm^{-3}. Solid line: Aldrich titanium dioxide. Broken line: Aldrich goethite.

25 titanium dioxide results could be improved. This is true only to some extent, because fouling of the reactor walls of radiation entrance with this catalyst is a serious problem [44]. It can be concluded, using a conservative argument, that the performance of goethite plus hydrogen peroxide is at least as good as that of titanium dioxide.

Looking at the LVRPA profiles as a function of the light penetration depth for both operations (Fig. 10) it can be seen that the distance where the photonic absorption rate becomes insignificant is at least one order of magnitude different. In the case of photocatalytic reactors, it is only necessary the minimum LVRPA required to reach the maximum activation of the employed semiconductor. Additionally, it is also needed the necessary surface area for reactants adsorption and the superficial reaction. Beyond these values, the excess concentration is even counterproductive (for Aldrich titanium dioxide this limit, under low to medium irradiation rates and very strong mixing operation, is about 2×10^{-3} g cm^{-3} [58,59]). This is so because the presence of a very large specific absorption coefficient forces to use thinner reactors in the characteristic direction of radiation propagation. This is exemplified by the innovative proposals of falling films and fountain film reactors, for example, but some of them are more difficult to operate under stable conditions resulting from the well-known film flow instabilities in the falling films [60–62]. Moreover, strong radiation absorption could lead to increase, beyond the required optimum concentrations, the existence of a large accumulation of electrons and holes in the surfaces of the catalytic particles positioned close to the wall of radiation entrance, favoring their recombination rates with the consequent lost of energy. Similarly, it is desired to have the minimum possible scattering (to avoid additional lost of photons). The extra difficulties associated with the possibility of mass

transfer control in concentrated catalytic suspensions subjected to high radiation absorption rates must also be considered.

At this point, from the results shown in Fig. 9 a conservative assumption can be made, considering that both reaction rates with titanium dioxide + UV and goethite with hydrogen peroxide + UV are of similar magnitude. This consideration even neglects the additional advantage of goethite whose radiation absorption can be extended into the visible region. The results obtained in this work can introduce a significant alteration in the concepts that could be involved in designing both types of reactors. The available light path length with goethite is much larger, permitting to reach significantly longer distances in the space of reaction where the catalyst can be efficiently activated.

It is possible to think of two practical annular reactors operated with the same lamps. This means that in both cases the radiation inlet boundary condition will be the same. The adopted catalyst loadings will be the same as described in the experiment corresponding to Fig. 9: 2×10^{-3} g cm^{-3}. In what follows two simple applications will be discussed.

8.1. Batch recycling reactors

One of the reactors is operated with TiO_2 catalyst and the other with the heterogeneous photo-Fenton catalyst plus hydrogen peroxide. In both cases, due to the particular characteristics of these reactions, since they are not very fast, both reactors could be operated as part of a closed circuit including a pump and a storage tank (Fig. 11).

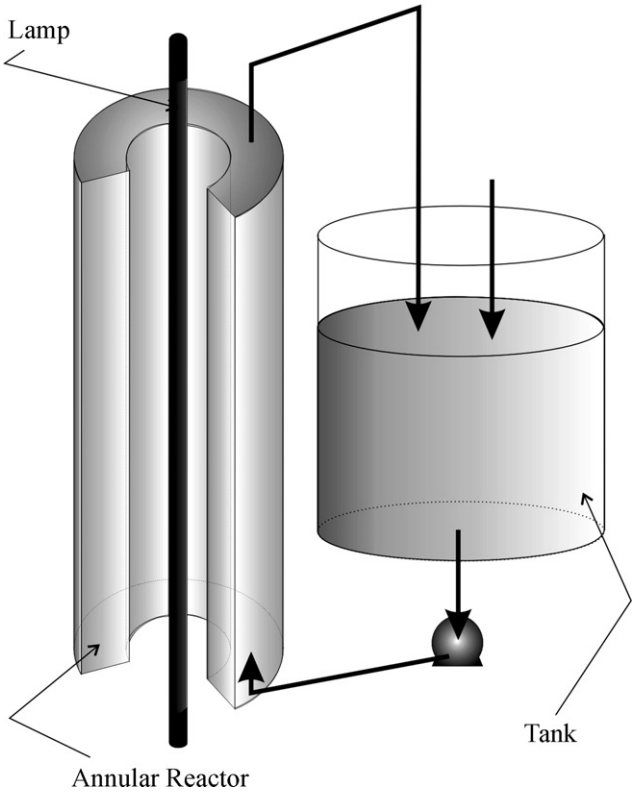

Fig. 11. Schematic representation of the annular reactor. Right arrow indicates oxygen intake or hydrogen peroxide intake according to the case.

Speaking in generic terms, a photochemical reaction kinetic model employing polychromatic radiation will be generally written in terms of a generalized functionality of this sort:

$$R_{\sum_\lambda} = R_{\sum_\lambda}[k(C_{2-CP})^{\alpha_1}, (C_{cm})^{\alpha_2}, (e^a_{\sum_\lambda})^{\alpha_3}, (C_{O_2})^{\alpha_4}, (C_{H_2O_2})^{\alpha_5}, \text{ pH, etc.}] \quad (29)$$

Notice that the effect of the absorbed light intensity for both reactions will be always present. Assume equivalent initial pollutant concentration (C^0_{2-CP}), the adoption of the optimum operating conditions for the other intervening variables in each process, including pH, and the previously discussed similar reaction rates. From Eqs. (4) and (29), it is clear that the value of the absorbed intensity to be included in the kinetic expression, will depend on the optical properties of the catalyst. These values will also define, as said before, the useful length in the characteristic direction of radiation propagation in the reactor. The effective radiation path length for both cases will be decisively different and the reaction space employing goethite can be much wider. This consideration, leads to the conclusion that for equal mean residence times to achieve the same conversion, the useful operating volume were radiation activation is efficient, will be significantly larger when using goethite. It must be noted that in addition, there is the contribution of the dark Fenton reaction occurring in the whole volume of the system, including the tank, in the case of the photo-Fenton process.

In the photocatalytic reactor with titanium dioxide, for catalyst concentrations in the order of 2×10^{-3} g cm^{-3} to avoid mass transfer limitations in the bulk of the fluid, it will be necessary to employ very large recirculation flow rates [58]. This operating condition will imply larger energy consumption in the pump.

Moreover, the reactor with the larger external diameter (with the obvious change in geometry from annular to cylindrical reactors) introduces the possibility of employing solar radiation in a more efficient way because the effective surface for collection of photons will be certainly largely improved. Furthermore, the high absorption rates with titanium dioxide will originate a square root dependence of the reaction rate with respect to the radiation absorption in some parts of the reactor volume [63] and, consequently, a lower TiO_2 photocatalytic reaction rate.

8.2. Continuous flow reactors

It could also be looked at the case of operating the process in continuous flow, annular reactors (Fig. 11, without the recycling system). In the case of the TiO_2 reactor, to avoid the foreseeable mass transfer limitations due to the very high photon absorption rates existing in the reaction space resulting from the very thick optical thickness, the reactor will have to be operated under very high flow rates. Consequently, in order to achieve the desired final conversion, several reactors in series will be required to process the pollutant flow rate according to the desired specifications. Again, as remarked before, the higher rate of recombination of electrons and holes at higher

radiation absorption levels will originate unwanted square root dependences with respect to the radiation absorption by the TiO_2 photocatalytic reactor. To complete the scenario, the downstream catalyst separation with the goethite catalyst will be much simpler.

8.3. Reactor efficiencies

It seems interesting to explore an additional concept: the total system efficiency [64,65]. Consider the following reactor efficiencies:

$$\eta_{Tot} = \eta_{Lamp}\eta_{Inc.}\eta_{Abs.}\eta_{Reac.}$$

where η_{Lamp}, $\eta_{Inc.}$, $\eta_{Abs.}$ and $\eta_{React.}$ are the energy efficiency of the lamp, the energy efficiency of the radiation incidence at the reactor wall, the radiation absorption efficiency, and the reaction overall quantum efficiency, respectively. It is certainly possible to assume that in a well-designed reactor the first three factors will be the same. In particular, the reactor thickness will be such that all the photon fluxes coming in will not escape from the reaction space due to the lack of sufficient radiation absorbing catalyst and/or reactor diameter. With this hypothesis, it is assigned to the supported titanium dioxide the same ability for collecting the incoming photons, in spite of the fact that due to its much larger scattering capabilities the real situation will be in favor of the goethite process. However, major differences will be observed in the fourth. The value of the reaction overall quantum efficiency, defined as:

$$\eta_{Reac.} = \frac{[\text{Amount of pollutant converted}]}{[\text{Amount of photons absorbed by the catalyst}]} \quad (31)$$

will be much larger in the heterogeneous photo-Fenton reaction than in the TiO_2 photocatalytic reaction. Two main causes can be mentioned: (i) for titanium dioxide reactors, due to the problem of mass transfer limitations in the bulk of the fluid, the amount of pollutant converted may be lower, and (ii) for normal irradiation rates, usually above one sun, having chemical reaction rates bearing a typical proportionality with the square root of the absorbed irradiation rate, the numerator may be much smaller in the TiO_2 reactor. Consequently, the total radiation energy efficiency will be larger in the heterogeneous photo-Fenton process.

9. Conclusions

A novel experimental method has been applied to characterize the optical properties of goethite suspensions as a function of wavelength. The method make uses of collimated transmittance measurements as well as diffuse transmittance and diffuse reflectance measurements. In this way, specific absorption coefficients, specific scattering coefficients and the asymmetry factor for the Henyey and Greenstein phase function were obtained in the range between 310 and 500 nm. Additionally, these results indicate that this catalyst is very appropriate to be used with solar radiation.

These suspensions were made with solid catalyst sizes between 100 and 200 meshes, allowing the possibility of working with particle dimensions that can be maintained in suspension, render reasonably good reaction rates and, at the same time, permitting a rapid sedimentation of the catalyst when the reaction is completed.

The obtained results, that are useful by themselves for kinetics studies and reactor design, bring about a conclusion of even greater significance. According to the measured optical properties, reactors using the goethite catalyst can have a much larger characteristic optical path length as compared with the most widely known photocatalytic reactions employing titanium dioxide. Several aspects concerning the economy of the process can be mentioned: (1) a larger flexibility in the choice of the best operating conditions and reactor configurations, (2) in the case of using solar reactors, a more effective ability for collecting and using the available radiation and (3) a higher total system efficiency.

Acknowledgements

The authors would like to thank Mr. Antonio Negro for his useful contributions in part of the experimental work. They are also grateful to Universidad Nacional del Litoral, Consejo Nacional de Investigaciones Científicas y Técnicas and Agencia Nacional de Promoción Científica y Tecnológica for their financial support. The technical assistance of Eng. Claudia Romani is also greatly acknowledged.

References

[1] J.P. Scott, D.F. Ollis, Integration of chemical and biological oxidation processes for water treatment: review and recommendations, Environ. Prog. 14 (1995) 88–103.
[2] V. Sarria, S. Parra, N. Adler, P. Peringer, N. Benitez, C. Pulgarin, Recent developments in the coupling of photoassisted and aerobic biological processes for the treatment of biorecalcitrant compounds, Catal. Today 76 (2002) 301–315.
[3] W. Gernjak, M. Fuerhacker, P. Fernández-Ibañez, J. Blanco, S. Malato, Solar photo-Fenton treatment-process parameters and process control, Appl. Cat. B: Environ. 64 (2006) 121–130.
[4] L.A. Pérez-Estrada, S. Malato, W. Gernjak, A. Agüera, M.E. Thurman, I. Ferrer, A.R. Fernández-Alba, Photo-Fenton degradation of diclofenac: identification of main intermediates and degradation pathway, Environ. Sci. Technol. 39 (2005) 8300–8306.
[5] A. Coelho, A.V. Castro, M. Dezotti, G.L. San't Anna Jr., Treatment of petroleum refinery sourwater by advanced oxidation processes, J. Hazard. Mater. B137 (2006) 178–184.
[6] Y. Sun, J.J. Pignatello, Photochemical reactions involved in the total mineralization of 2,4-D by Fe^{+3}/H_2O_2/UV, Environ. Sci. Technol. 27 (1993) 304–310.
[7] S.H. Bossmann, E. Oliveros, S. Gob, S. Siegwart, E.P. Dahlen, L. Payawan, M. Staub, M. Worner, A.M. Braun, New evidence against hydroxyl radicals as reactive intermediates in the thermal and photochemically enhanced Fenton reactions, J. Phys. Chem. 102 (1998) 5542–5550.
[8] J. De Laat, H. Gallard, Catalytic decomposition of hydrogen peroxide by Fe(III) in homogeneous aqueous solution: mechanism and kinetic modelling, Environ. Sci. Technol. 33 (1999) 2726–2732.
[9] J.J. Pignatello, D. Liu, P. Huston, Evidence for an additional oxidant in the photoassisted Fenton reaction, Environ. Sci. Technol. 33 (1999) 1832–1839.
[10] S. Malato, J. Blanco, A. Vidal, D. Alarcón, M. Maldonado, J. Cáceres, W. Gernjak, Applied studies in photocatalytic detoxification: an overview, Sol. Energy 75 (2003) 329–336.

[11] G.H. Rossetti, E.D. Albizzati, O.M. Alfano, Modeling of a flat-plate solar reactor. Degradation of formic acid by the photo-Fenton reaction, Sol. Energy 77 (2004) 461–470.
[12] J. Fernandez, J. Bandara, A. Lopez, P. Albersc, J. Kiwi, Efficient photo-assisted Fenton catalysis mediated by Fe ions on nafion membranes active in the abatement of non-biodegradable azo-dye, Chem. Commun. (1998) 1493–1494.
[13] J. Fernandez, J. Bandara, A. Lopez, Ph. Buffat, J. Kiwi, Photoassisted Fenton degradation of nonbiodegradable azo dye (orange II) in Fe-free solutions mediated by cation transfer membranes, Langmuir 15 (1999) 185–192.
[14] S. Parra, I. Guasquillo, O. Enea, J. Mielczarski, P. Albers, L. Kiwi-Minsker, J. Kiwi, Abatement of an azo dye on structured C-nafion/Fe-ion surfaces by photo-Fenton reactions leading to carboxylate intermediates with a remarkable biodegradability increase of the treated solution, J. Phys. Chem. B 107 (2003) 7026–7035.
[15] J. Fernandez, M.R. Dhananjeyan, J. Kiwi, Y. Senuma, J. Hilborn, Evidence for Fenton photoassisted processes mediated by encapsulated Fe ions at biocompatible pH values, J. Phys. Chem. B 104 (2000) 5298–5301.
[16] A. Bozzi, T. Yuranova, J. Mielczarski, J. Kiwi, Abatement of oxalates catalyzed by Fe-silica structured surfaces via cyclic carboxylate intermediates in photo-Fenton reactions, Chem. Commun. 19 (2002) 2202–2203.
[17] A. Bozzi, T. Yuranova, J. Mielczarski, J. Kiwi, Evidence for immobilized photo-Fenton degradation of organic compounds on structured silica surfaces involving Fe recycling, New J. Chem. 28 (2004) 519–526.
[18] M. Nematu, C. Zaharia, C. Catrinescu, A. Yediler, M. Macoveanu, A. Kettrup, Fe-exchanged Y zeolite as catalyst for wet peroxide oxidation of reactive azo dye procion marine H-EXL, App. Catal. B: Environ. 48 (2004) 287–294.
[19] M. Noorjahn, V. Durga Kumari, M. Subrahmanyan, L. Panda, Immobilized Fe(III)-HY: an efficient and stable photo-Fenton catalyst, App. Catal. B: Environ. 57 (2004) 289–296.
[20] Z.W. Zheng, L.C. Lei, S.J. Xu, P. Cen, Heterogeneous UV/Fenton catalytic degradation of wastewater containing phenol with Fe-Cu-Mn-Y catalyst, J. Zhjiang Univ. Sci. 58 (2004) 206–211.
[21] J. Feng, X. Hu, P.L. Yue, Degradation of azo-dye orange II by a photoassisted Fenton reaction using a novel composite if iron oxide and silicate nanoparticles as a catalyst, Ind. Eng. Chem. Res. 42 (2003) 2058–2066.
[22] J. Feng, X. Hu, P.L. Yue, Discoloration and mineralization of orange II by using a bentonite clay-based Fe nanocomposite film as a heterogeneous photo-Fenton catalyst, Water Res. 39 (2005) 89–96.
[23] A. Cuzzola, M. Bernini, P. Salvadori, A preliminary study on iron species as heterogeneous catalysts for the degradation of linear alkylbenzene sulphonic acids by H_2O_2, Appl. Catal. B: Environ. 36 (2002) 231–237.
[24] T. Yuranova, O. Enea, E. Mielczarski, J. Mielczarski, P. Albers, J. Kiwi, Fenton immobilized photo-assisted catalysis through a Fe/C structured fabric, Appl. Catal. B: Environ. 49 (2004) 39–50.
[25] S. Chou, C. Huang, Y.H. Huang, Heterogeneous and homogeneous catalytic oxidation by supported gamma-FeOOH in a fluidized-bed reactor: kinetic approach, Environ. Sci. Technol. 35 (2001) 1247–1251.
[26] J. Feng, X. Hu, P.L. Yue, Discoloration and mineralization of orange II using different heterogeneous catalysts containing Fe: a comparative study, Environ. Sci. Technol. 38 (2004) 5773–5778.
[27] Martínez, G. Calleja, J.A. Melero, R. Molina, Heterogeneous photo-Fenton degradation of phenolic aqueous solutions over iron-containing SBA-15 catalyst, Appl. Catal. B: Environ. 60 (2005) 181–190.
[28] Martínez, G. Calleja, J.A. Melero, R. Molina, Iron species incorporated over different silica supports for the heterogeneous photo-Fenton oxidation of phenol, Appl. Catal. B: Environ. 70 (2007) 452–460.
[29] S.S. Lin, M.D. Gurol, Heterogeneous catalytic oxidation of organic compounds by hydrogen peroxide, Water Sci. Technol. 34 (1996) 57–64.
[30] S.S. Lin, M.D. Gurol, Catalytic decomposition of hydrogen peroxide on iron oxide: kinetics, mechanism and implications, Environ. Sci. Technol. 32 (1998) 1417–1423.
[31] M.D. Gurol, S.S. Lin, Hydrogen peroxide/iron oxide-induced catalytic oxidation of organic compounds, Water Sci. Technol.: Water Supply 1 (2001) 131–138.
[32] Lu Ming-Chun, Oxidation of chlorophenols with hydrogen peroxide in the presence of goethite, Chemosphere 40 (2000) 125–130.
[33] A. Teel, C.R. Warberg, D.A. Atkinson, R.J. Watts, Comparison of mineral and soluble iron Fenton's catalyst for the treatment of trichloroethylene, Water Res. 35 (2001) 984–997.
[34] R. Andreozzi, V. Caprio, R. Marotta, Oxidation of 3,4-dihydroxybenzoic acid by means of hydrogen peroxide in aqueous goethite slurry, Water Res. 36 (2002) 2761–2768.
[35] J. He, W. Ma, J. He, J. Zhao, J.C. Yu, Photooxidation of azo dye in aqueous dispersions of H_2O_2/alfa-FeOOH, Appl. Catal. B: Environ. 39 (2002) 211–220.
[36] J. He, W. Ma, W. Song, J. Zhao, X. Qian, S. Zhang, J.C. Yu, Photoreaction of aromatic compounds at alfa-FeOOH/H_2O interface in the presence of H_2O_2: evidence for organic-goethite surface complex formation, Water Res. 39 (2005) 119–128.
[37] M. Kosmulski, E. Maczka, Z. Jartych, J.B. Rosaholm, Synthesis and characterization of goethite and goethite–hematite composite: experimental study and literature survey, Adv. Colloid Interface 103 (2003) 57–76.
[38] P. Kubelka, F. Munk, Ein Beitrag zur Optik der Farbanstriche, Z. Tech. Phys. 12 (1931) 593–601. Quoted from: Ciani et al., 2005.
[39] A. Ciani, K.U. Goss, R.P. Schwarzenbach, Light penetration in solid and particulate minerals, Eur. J. Soil Sci. 56 (2005) 561–573.
[40] M.N. Ozisik, Radiative Transfer and Interactions with Conduction and Convection, J. Wiley, New York, 1973.
[41] A.E. Cassano, C.A. Martín, R.J. Brandi, O.M. Alfano, Photoreactor analysis and design: fundamentals and applications, Ind. Eng. Chem. Res. 34 (1995) 2155–2220.
[42] M.I. Cabrera, O.M. Alfano, A.E. Cassano, Absorption and scattering coefficients of titanium dioxide particulate suspensions in water, J. Phys. Chem. 100 (1996) 20043–20050.
[43] R.J. Brandi, O.M. Alfano, A.E. Cassano, Rigorous model and experimental verification of the radiation field in a flat-plate solar collector simulator employed for photocatalytic reactions, Chem. Eng. Sci. 54 (1999) 2817–2827.
[44] R.L. Romero, O.M. Alfano, A.E. Cassano, Radiation field in an annular. Slurry photocatalytic reactor. 2. Model and experiments, Ind. Eng. Chem. Res. 42 (2003) 2479–2488.
[45] M.L. Satuf, R.L. Brandi, A.E. Cassano, O.M. Alfano, Experimental method to evaluate the optical properties of aqueous titanium dioxide suspensions, Ind. Eng. Chem. Res. 44 (2005) 6643–6649.
[46] H.C. Van de Hulst, Multiple Light Scattering, Academic Press, 1980 (Chapter 10).
[47] J. Marugan, R. Van Grieken, O.M. Alfano, A.E. Cassano, Optical and physicochemical properties of silica-supported TiO_2 photocatalyst, AIChE J. 52 (2006) 2832–2843.
[48] J.J. Duderstadt, R. Martin, Transport Theory, J. Wiley, New York, 1979 (Chapter 8).
[49] G. Spadoni, E. Bandini, F. Santarelli, Scattering effects in photosensitized reactions, Chem. Eng. Sci. 33 (1978) 517–524.
[50] M. Pasquali, F. Santarelli, J.F. Porter, P.L. Yue, Radiative transfer in photocatalytic systems, AIChE J. 42 (1996) 532–537.
[51] Q. Yang, P.L. Ang, M.B. Ray, S.O. Pahkonen, Light distribution field in catalyst suspensions within an annular photoreactor, Chem. Eng. Sci. 60 (2005) 5255–5268.
[52] O.M. Alfano, A.C. Negro, M.I. Cabrera, A. Cassano, Scattering effects produced by inert particles in photochemical reactors. 1. Model and experimental verification, Ind. Eng. Chem. Res. 34 (1995) 488–499.
[53] R.J. Brandi, O.M. Alfano, A.E. Cassano, Modeling of radiation absorption in a flat plate photocatalytic reactor, Chem. Eng. Sci. 51 (1996) 3169–3174.
[54] R.L. Romero, O.M. Alfano, A.E. Cassano, Cylindrical photocatalytic reactors. Radiation absorption and scattering effects produced by suspended fine particles in an annular space, Ind. Eng. Chem. Res. 36 (1997) 3094–3109.
[55] G. Sgalari, G. Camera-Roda, F. Santarelli, Discrete ordinate method in the analysis of radiative transfer in photocatalytically reacting media, Int. Commun. Heat Mass Transfer 25 (1998) 651–660.
[56] K.A. Levenberg, Method for the solution of certain problems in least squares, Q. Appl. Math. 2 (1944) 164–168.

[57] D. Marquardt, An algorithm for least-squares estimation of nonlinear parameters, SIAM J. Appl. Math. 11 (1963) 431–441.
[58] M.M. Ballari, R.J. Brandi, O.M. Alfano, A.E. Cassano, Mass transfer limitations in photocatalytic reactors employing titanium dioxide suspensions. I. Concentration profiles in the bulk, Chem. Eng. J. 136 (2008) 50–65.
[59] M.M. Ballari, R.J. Brandi, O.M. Alfano, A.E. Cassano, Mass transfer limitations in photocatalytic reactors employing titanium dioxide suspensions. II. External and internal particle constrains for the reaction, Chem. Eng. J. 136 (2008) 242–255.
[60] G. Li Puma, P.L. Yue, A novel fountain photocatalyic reactor for water treatment and purification: modelling and design, Ind. Eng. Chem. Res. 40 (2001) 5162–5169.
[61] G. Li Puma, P.L. Yue, Modelling and design of thin-film slurry photocatalytic reactors for water purification, Chem. Eng. Sci. 58 (2003) 2269–2281.
[62] G. Li Puma, Modelling of thin-film slurry photocatalytic affected by radiation scattering, Environ. Sci. Technol. 37 (2003) 5783–5791.
[63] O.M. Alfano, M.I. Cabrera, A. Cassano, Photocatalytic reactions involving hydroxyl radical attack. 1. Reaction kinetics formulation with explicit photon absorption effects, J. Catal. 172 (1997) 370–379.
[64] J. Cerdá, J.L. Marchetti, A.E. Cassano, Radiation efficiencies in elliptical photoreactors, Latin Am. J. Heat Mass Transfer 1 (1977) 33–63.
[65] G.E. Imoberdorf, A.E. Cassano, H.A. Irazoqui, O.M. Alfano, Simulation of a multi-annular photocatalytic reactor for degradation of perchloroethylene in air. Parametric analysis of radiative energy efficiencies, Chem. Eng. Sci. 62 (2007) 1138–1154.